Flip-Flopping Binary Black Holes

Carlos O. Lousto and James Healy

Flip-flopping binary black holes

Carlos O. Lousto and James Healy

Center for Computational Relativity and Gravitation,
School of Mathematical Sciences, Rochester Institute of Technology,
85 Lomb Memorial Drive, Rochester, New York 14623
(Dated: March 18, 2015)

We study binary spinning black holes to display the long term individual spin dynamics. We perform a full numerical simulation starting at an initial proper separation of $d \approx 25M$ between equal mass holes and evolve them down to merger for nearly 48 orbits, 3 precession cycles, and half of a flip-flop cycle. The simulation lasts for $t = 20000M$ and displays a total change in the orientation of the spin of one of the black holes from initially aligned with the orbital angular momentum to a complete anti-alignment after half of a flip-flop cycle. We compare this evolution with an integration of the 3.5 Post-Newtonian equations of motion and spin evolution to show that this process continuously flip-flops the spin during the lifetime of the binary until merger. We also provide lower order analytic expressions for the maximum flip-flop angle and frequency. We discuss the effects this dynamics may have on spin growth in accreting binaries and on the observational consequences for galactic and supermassive binary black holes.

Introduction: Numerical relativity techniques are now able to directly simulate binary black hole mergers [1–3]. In particular one can follow the dynamics of black hole spins in an inspiral orbit down to the formation of the final remnant black hole [4]. One of the most striking results of those studies has been the discovery of very large recoil velocities [5] acquired by the merger remnant, up to $5000 km/s$ [6] for hangup configurations.

It has been pointed out [7] that the presence of accreting matter can align (or counter align) spins with the orbital angular momentum thus reducing the recoil velocities to a few hundred km/s [8]. Recent studies of the tidal effects on tilted accretion disks around spinning black holes find almost perfect alignments of the spins with the orbital angular momentum [9, 10] on a shorter time scale than that of gravitational radiation (for black hole separations above a thousand gravitational radii).

While those studies have been performed on individual black holes, we revisit this scenario to study the precession dynamics of black hole spins in a binary system. In particular we are interested in the dynamics of polar precession of each individual spin. We find a flip-flop mode with periods shorter than the gravitational radiation scale and with relatively high probability to occur given generic (but comparable mass) initial configurations. We briefly discuss the effects that this flip-flopping spin could have on the inner accretion disk dynamics and its potential observational consequences.

Full Numerical Evolution: In order to display the long term dynamics of spinning binary black holes in General Relativity we start a numerical simulation at a proper separation $d \approx 25M$. We study an equal mass binary with different spin magnitudes and orientations. In particular, we choose one of the black holes as slowly spinning with its spin $\vec{S}_1$ initially aligned with the orbital angular momentum $\vec{L}$, while the second highly spinning black hole has spin $\vec{S}_2$ lying mostly along the orbital plane, but slightly anti-aligned with $\vec{L}$, such that the total spin $\vec{S}$ exactly lies in the orbital plane, i.e. $\vec{S} \cdot \vec{L} = 0$. These choices (See Table I) are for the sake of simplicity of the analysis, and also provide a plausible scenario where accretion has proceeded to align one of the black holes with $\vec{L}$ and led to comparable masses by preferably accreting onto the initially smaller hole [11]. We also choose the magnitude of the first black hole to be smaller than that of the second, foreseeing (as discussed later in this paper) that the flip-flopping spin neutralizes (at least partially) the growth of intrinsic spin magnitudes, $S_{1,2}/m_{1,2}^2$, by accretion.

We use the TwoPunctures thorn [12], a spectral numerical code to generate initial "puncture" (no excision of the horizon) data for the binary black hole simulations. We evolve these initial data sets using the LazEv [13] implementation of the moving puncture approach [2]. For the runs presented here, we use centered, eighth-order finite differencing in space [14] and a fourth-order Runge Kutta time integrator. Our code uses the Cactus/EinsteinToolkit [15, 16] infrastructure for parallelization. We use the Carpet [17] mesh refinement driver to provide a "moving boxes" style of mesh refinement. We locate the apparent horizons using the AHFinderDirect code [18] and measure the horizon spin using the isolated horizon algorithm detailed in [19]. For the computation of the radiated energy and linear momentum we use the asymptotic formulas in [20] which are expressed directly in terms of the Weyl scalar ψ_4.

To complete the full evolution required 2.5 million service units on 25 to 30 nodes of our local cluster "Blue Sky" with dual Intel Xeon E5-2680 processors nearing $100M$ of evolution per day. Our evolution is free and we

TABLE I. Initial data parameters and system details. The punctures are located at $\vec{r}_1 = (x_1, 0, z)$ and $\vec{r}_2 = (x_2, 0, z)$, with momenta $P = \pm(0, P, 0)$, spins $\vec{S}_1 = (0, 0, S_{1z})$ and $\vec{S}_2 = (S_{2x}, 0, S_{2z})$, mass parameters m^p, horizon (Christodoulou) masses m^H, total ADM mass M_{ADM}, and dimensionless spins $\alpha = a/m_H = S/m_H^2$. The horizon masses and spins are given after the gauge settles, and the errors in m^H and α are determined by the drift in the quantity during the inspiral. Also provided are the simple proper distance d, eccentricity at the start of the inspiral e_i, and eccentricity e_f and the number of orbits N just before merger.

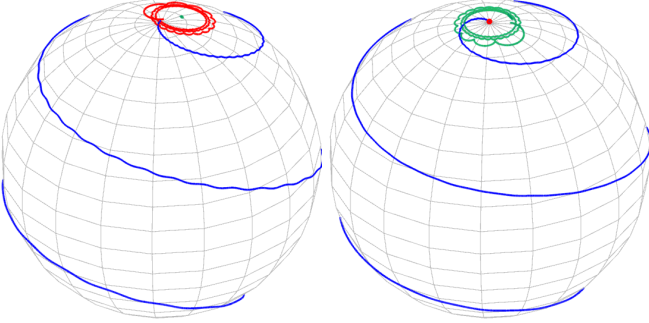| x_1/m	x_2/m	z/m	P/m	d/m
10.73983	-10.76016	-0.01968	0.05909	25.37
m_1^p/m	m_2^p/m	S_{1z}/m^2	S_{2x}/m^2	S_{2z}/m^2
0.48543	0.30697	0.05	0.19365	-0.05
M_{ADM}/m	J_{ADM}/m^2	e_i	e_f	N
0.99472	1.2704344	0.0322	0.0006	48.5
m_1^H/m	$\delta m_1^H/m$	m_2^H/m	$\delta m_2^H/m$	
0.50000	0.00002	0.49974	0.00001	
α_1	$\delta\alpha_1$	α_2	$\delta\alpha_2$	
0.20003	0.00056	0.80088	0.00066	

FIG. 1. Directional evolutions of the spins and angular momentum in the initial coordinate frame (left) and in the non-inertial $\vec{L}$ frame (right). Color Keys: red $\hat{L}$, green $\hat{J}$, blue $\hat{S}_1$.

verify its accuracy by the satisfaction of the Hamiltonian and Momentum constraints. All four L_2-norm quantities remain well below 10^{-8} until merger. Individual horizon masses m_1^H and m_2^H are preserved to a level of 2 and 1.4 parts in 10^5 respectively until merger. Spins grow linearly with time until merger by a total increase of 1.5×10^{-4}. Thus the total increase of the intrinsic spin magnitudes $\alpha_{1,2} = S_{1,2}/m_{1,2}^2$ are $\delta\alpha_1 = 6 \times 10^{-4}$ and $\delta\alpha_2 = 6 \times 10^{-4}$ from initial data to merger, as described in Table I.

The azimuthal precessional effect and polar flip-flop can be directly seen in the evolution of the spin components of the black holes represented over a sphere in Fig. 1. The effect is apparent in the frame of the orbital plane as well as the fixed initial set of coordinates.

Fig. 2 displays the angles that the (slower spinning) black hole spin $\vec{S}_1$ forms with the precessing orbital an-
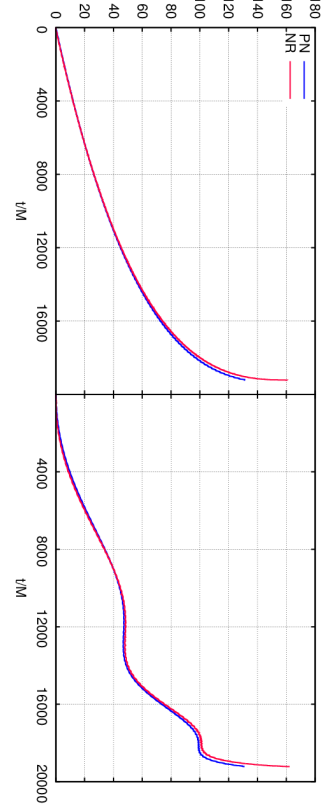

FIG. 2. The angle between the spin of the secondary (smaller spin) black hole $\vec{S}_1$ with respect to the orbital angular momentum $\vec{L}$ (left) and with respect to the fixed z-axis (right). For comparison we also plot the 3.5PN prediction, which underestimates the flip of the angle at the latest stages of evolution (merger).

gular momentum $\vec{L}$ or with the fixed $\hat{z}$-axis as a function of time. Both start originally aligned and by the time of merger both display an almost total flip, around $160°$. Had we started the binary further separated apart this spin would continue to flip-flop between complete alignment and counter alignment as described in the next section using the Post-Newtonian (PN) approximation. We also compare our results with the corresponding 3.5PN integration of the equations of motion and spin evolution [21, 22]. We observe a long initial superposition of the PN and full numerical precession curves corresponding to the early $15000M$ of evolution, when the the binary's separations is above around $15M$. As the merger proceeds and the evolution becomes more dynamical we observe larger deviations from each other, with the numerical solution to General Relativity presenting a stronger spin-flip effect.

Fig. 3 displays the leading waveform modes for the strain. In the top panel is the characteristic chirp of the $(\ell, m) = (2, 2)$ mode, with an increasing amplitude slightly modulated at around the orbital frequency due
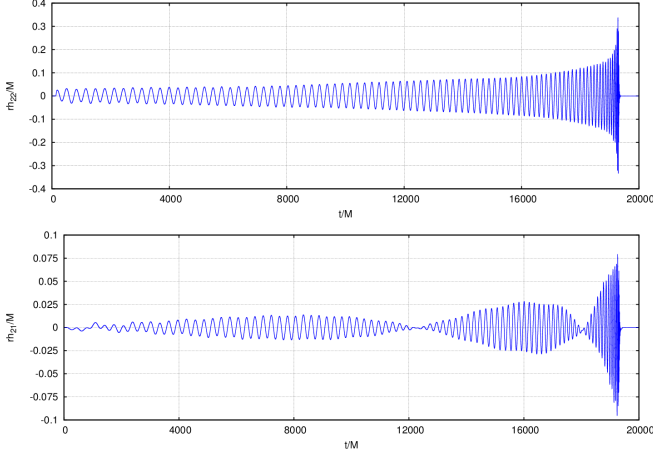
FIG. 3. The real part of the waveform strain for the modes $(\ell, m) = (2, 2)$ and $(\ell, m) = (2, 1)$. While the former (top) gives the leading chirping amplitude, the latter (bottom) clearly displays the precession effect, completing nearly three cycles during the $t = 20000M$ of the simulation.

TABLE II. Remnant properties and recoil velocity. The final mass and spin are measured from the horizon, and the recoil velocity is calculated from the gravitational waveforms. The error in the mass and spin is determined by the drift in those quantities after the remnant settles down. The error in the recoil velocity is the difference between first and second order polynomial extrapolation to infinity.

M_{rem}/m	$|\alpha_{rem}|$	$V_{recoil}[km/s]$
0.94904 ± 0.00000	0.70377 ± 0.00002	1508.49 ± 16.08
α_{rem}^x	α_{rem}^y	α_{rem}^z
0.10815 ± 0.00003	-0.01986 ± 0.00000	0.69513 ± 0.00002

to the nutation of $\vec{L}$ around the total angular momentum $\vec{J}$ (See Fig. 1 in Ref. [23]). The lower panel shows the azimuthal precessional effect of $\vec{L}$ on the amplitude of the $(2, 1)$ mode, showing (in a gauge invariant way) that we evolved for nearly three precessional cycles (See Ref. [24] for a first discussion relating this mode to precession in full numerical simulations).

Table II displays the properties of the final black hole remnant formed after merger. Notably, the recoil reaches $1500km/s$, and the orientation of the final spin changes by only 1.62 degrees with respect to the initial direction of the total angular momentum, as expected for comparable mass binaries [25, 26].

Post Newtonian spin dynamics: In order to provide an analytic understanding of the flip-flop spin mode, we look at the precession equations for the spins $\vec{S}_1$ and $\vec{S}_2$ with a mass ratio $q = m_1/m_2$ to leading spin-orbit and spin-spin couplings in the (2PN) post-Newtonian expansion [22]

$$\frac{d\vec{S}_1}{dt} = \frac{1}{r^3} \left[\left(2 + \frac{3}{2q}\right) \vec{L} - \vec{S}_2 + \frac{3(\vec{S}_0 \cdot \hat{n})}{1 + q} \hat{n} \right] \times \vec{S}_1,$$
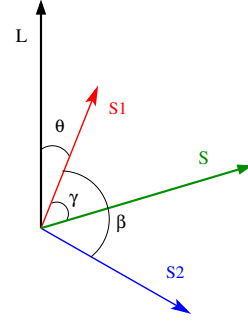

FIG. 4. Spin configurations $\vec{S}_1$ and $\vec{S}_2$ relative to the orbital angular momentum $\vec{L}$. Here $\vec{S} = \vec{S}_1 + \vec{S}_2$.

$$\frac{d\vec{S}_2}{dt} = \frac{1}{r^3} \left[\left(2 + \frac{3q}{2}\right) \vec{L} - \vec{S}_1 + \frac{3q(\vec{S}_0 \cdot \hat{n})}{1 + q} \hat{n} \right] \times \vec{S}_2, (1)$$

where $\vec{n} = \vec{r}_1 - \vec{r}_2$ and

$$\vec{S}_0 = \left(1 + \frac{1}{q}\right) \vec{S}_1 + (1 + q)\vec{S}_2. \tag{2}$$

For more details see the reviews in Refs. [27, 28].

For direct connection with the full numerical simulation above we will consider here the equal mass case, i.e. $q = 1$ and for the sake of simplicity, the conservative 2PN spin dynamics at fixed r. We next consider a generic configuration of binary black holes with arbitrary spins $\vec{S}_1$ and $\vec{S}_2$ at an angle β with respect to each other and adding up to the vector $\vec{S}$. For definiteness $\vec{S}_1$ is the spin of the black hole 1 at an angle γ with respect to $\vec{S}$ as shown in Fig. 4 and $\vec{S}_2$ is the spin of the black hole 2 identified with the larger spin magnitude S_2.

From Eqs. (1) the magnitude of the individual spins S_1 and S_2 are conserved as well as the magnitude of its sum, S (This has been observed to be approximately true in full nonlinear simulations of binary black holes solving General Relativity field equations numerically [29]). It follows that the following quantities are conserved:

$$\vec{S} \cdot \vec{S} = S^2 = S_1^2 + S_2^2 + 2S_1 S_2 \cos\beta = \text{constant}, (3)$$
$$\vec{S} \cdot \vec{S}_1 = SS_1 \cos\gamma = S_1^2 + S_2 S_1 \cos\beta = \text{constant}. (4)$$

In turn, this leads to the conservation of β and γ during the evolution of the binary. In particular we find that $\vec{S}_1$ oscillates around $\vec{S}$ between polar angles γ and $-\gamma$ (when it is both coplanar to $\vec{S}$ and $\vec{L}$). We call this the *flip-flop* angle

$$\theta_{ff} = \theta_{max} - \theta_{min} = 2\gamma, \tag{5}$$

where

$$\cos\gamma = \frac{S_1 + S_2 \cos\beta}{\sqrt{S_1^2 + S_2^2 + 2S_1 S_2 \cos\beta}} = \frac{S^2 + S_1^2 - S_2^2}{2SS_1}. \tag{6}$$

By decomposing the spin evolution equations (1) along $\vec{L}$ and perpendicular to it, in the fashion of [26],

Sec. IV.A, we obtain equations of the form $d(\vec{S}_i \cdot \hat{L})/dt = \Omega_{ff} \vec{S}_i \cdot \hat{L} + ...$ for $i = 1, 2$ and analogously for the perpendicular component of S_i giving Ω_p. From where we can read-off the average polar and azimuthal oscillations frequencies of the spin $\vec{S}_1$ (See also [30])

$$\Omega_{ff} = 3\frac{S}{r^3}\left[1 - \frac{2\vec{S}\cdot\hat{L}}{M^{3/2}r^{1/2}}\right], \qquad (7)$$

$$\Omega_p = \frac{7L}{2r^3} + \frac{2}{r^3}(\vec{S}\cdot\hat{L}). \qquad (8)$$

that we identify with the flip-flop and precession frequencies respectively.

Note that the black hole 2 also oscillates at this Ω_{ff} frequency, but with a smaller flip-flop angle (Since $S_2 > S_1$) given by $2(\beta - \gamma)$ where

$$\cos(\beta - \gamma) = \frac{S^2 + S_2^2 - S_1^2}{2SS_2}. \qquad (9)$$

Thus both spins, $\vec{S}_1$ and $\vec{S}_2$, oscillate around $\vec{S}$ which in turn precess around $\vec{L}$.

This oscillation of the spins represent a *genuine* spin-flip in the sense that it is the same object that completely changes its spin orientation. This is different from the simple case where the final remnant spin has flipped direction when compared to the spin of one of the individual orbiting black holes [31].

Discussion: In the scenario of binary black holes carrying individual thin accretion disks (and possibly a common circumbinary disk), spins changing their orientation can generate dramatic dynamical effects on the accreting matter around them. For definiteness, we focus on the black hole with spin $\vec{S}_1$ undergoing direction changes, which when viewed in the orbital frame, resembles the peeling of an orange (See Fig. 1). Due to the relatively short time scale of flip-flop at close separations, the accreting matter increases the black hole spin during half the flip-flop period, but decreases it during the other half. On the other hand, mass is always added to the black holes during both the up and down states. The resulting net effect is to lower the intrinsic spin magnitude, S_1/m_1^2.

From Eqs. (6) and (7), which represent a good approximation for well separated binaries ($r >> 100M$), requiring a flip-flop angle of 180° implies that $\gamma = \pi/2$ and $\Omega_{ff} = 3\sqrt{S_2^2 - S_1^2}/r^3$. For a maximally spinning hole 2 and a hole 1 with a relatively small spin at $1000M$ of separation, we obtain a flip-flop period

$$T_{ff} = \frac{2\pi}{\Omega_{ff}} = 32,700\,yr\left(\frac{r}{1000M}\right)^3\left(\frac{M}{10^8 M_\odot}\right), \quad (10)$$

which is shorter (by a factor of 40) than the gravitational radiation periods reported in [9] used to compare with the accretion-driven alignment mechanisms [32]. We thus conclude that such alignment processes might be less effective than expected when the flip-flop of spins is taken into account.
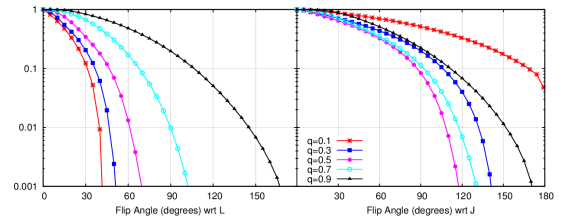

FIG. 5. The probability of a spin flip-flop angle $\theta_{ff} \geq x$ for a given mass ratio q and assuming random spin orientations and magnitudes of the primary and secondary black holes.

These flip-flop configurations might be very effective at disrupting the inner accretion disk dynamics and at circumventing the spin alignment (and growth) process by accretion, thus leading to important observational consequences. For instance, the change of the location of the internal rim of the disk due to the flip of the spin will change the high frequencies end of fluctuations and the electromagnetic spectrum due to changes in the efficiency of the conversion of the accreting flow, i.e. proportional to $E_{ISCO}(\pm a)$. Flip-flopping spins might also generate turbulent accretion by changing the stirring leading to increase/decrease of the radiation (See [33]). These examples provide rough estimates of the disrupting effects of a flip-flopping spin and a more accurate evaluation requires a full numerical magnetohydrodynamic simulation of such binary black hole configurations. Our full numerical run proves that, although demanding, these simulations are currently possible and they can be performed adding a magnetohydrodynamic description of the matter on a dynamical binary black hole background [34].

The change in the spin orientation at the latest stage of the merger could be followed through detailed observation of the gas jets in X-shaped radio galaxies [35]. The time scale for this phenomena, for instance, for the $\sim 25000M$ semiperiod we observe for the flip-flop in our full numerical simulation, corresponds to 1.2 seconds for $10 M_\odot$ binaries and 142 days for $10^8 M_\odot$ binaries. Note that according to Eq. (7) frequencies can be even higher if the black hole 2 would be closer to maximally spinning.

To appreciate the astrophysical relevance of this phenomenon it is important to determine the likelihood of these flip-flop angles out of all possible generic binary black hole merger configurations. We hence consider binaries with different mass ratios, q, and initial random spins α_1, $\cos(\theta_1)$, α_2, $\cos(\theta_2)$, with $\phi_1 - \phi_2 = 0, \pi$ (this last piece due to the resonances studied in [36–38]). We evolve these configurations from separations $r = 100M$ down to $r = 5M$, representing merger, using the 3.5 post-Newtonian approximation. The results of 2,922,656 simulations per q displaying the probability of a flip-flop angle larger than x are summarized in Fig. 5. The spin-flip angles remain large for comparable masses and this phenomena may also occur, to a lesser extent, in black hole

- neutron stars binaries. Note that accretion onto black hole binaries tends to bring the mass ratio towards 1 because the smaller hole is further away from the center of mass of the system and can sweep out more mass from the internal parts of the circumbinary accretion disk [11]. The flip-flop frequency for large binary separations and $q \neq 1$ is given by $\Omega_{ff}(q) \approx (3/2)(1-q)/(1+q)(M/r)^{-5/2}$. A thorough study of the unequal mass binary regime is being completed and will be published by the authors elsewhere.

[1] F. Pretorius, Phys. Rev. Lett. **95**, 121101 (2005), gr-qc/0507014.

[2] M. Campanelli, C. O. Lousto, P. Marronetti, and Y. Zlochower, Phys. Rev. Lett. **96**, 111101 (2006), gr-qc/0511048.

[3] J. G. Baker, J. Centrella, D.-I. Choi, M. Koppitz, and J. van Meter, Phys. Rev. Lett. **96**, 111102 (2006), gr-qc/0511103.

[4] M. Campanelli, C. O. Lousto, and Y. Zlochower, Phys. Rev. **D74**, 041501(R) (2006), gr-qc/0604012.

[5] M. Campanelli, C. O. Lousto, Y. Zlochower, and D. Merritt, Astrophys. J. **659**, L5 (2007), gr-qc/0701164.

[6] C. O. Lousto and Y. Zlochower, Phys. Rev. Lett. **107**, 231102 (2011), arXiv:1108.2009 [gr-qc].

[7] T. Bogdanovic, C. S. Reynolds, and M. C. Miller, Astrophys. J. **661**, L147 (2007), arXiv:astro-ph/0703054.

[8] J. Healy, C. O. Lousto, and Y. Zlochower, (2014), arXiv:1406.7295 [gr-qc].

[9] M. Coleman Miller and J. H. Krolik, Astrophys. J. **774**, 43 (2013), arXiv:1307.6569 [astro-ph.HE].

[10] K. A. Sorathia, J. H. Krolik, and J. F. Hawley, Astrophys. J. **777**, 21 (2013), arXiv:1309.0290 [astro-ph.HE].

[11] B. D. Farris, P. Duffell, A. I. MacFadyen, and Z. Haiman, Astrophys. J. **783**, 134 (2014), arXiv:1310.0492 [astro-ph.HE].

[12] M. Ansorg, B. Brügmann, and W. Tichy, Phys. Rev. **D70**, 064011 (2004), gr-qc/0404056.

[13] Y. Zlochower, J. G. Baker, M. Campanelli, and C. O. Lousto, Phys. Rev. **D72**, 024021 (2005), arXiv:gr-qc/0505055.

[14] C. O. Lousto and Y. Zlochower, Phys. Rev. **D77**, 024034 (2008), arXiv:0711.1165 [gr-qc].

[15] Cactus Computational Toolkit home page: http://cactuscode.org.

[16] F. Loffler, J. Faber, E. Bentivegna, T. Bode, P. Diener, *et al.*, Class. Quant. Grav. **29**, 115001 (2012), arXiv:1111.3344 [gr-qc].

[17] E. Schnetter, S. H. Hawley, and I. Hawke, Class. Quant. Grav. **21**, 1465 (2004), gr-qc/0310042.

[18] J. Thornburg, Class. Quant. Grav. **21**, 743 (2004), gr-qc/0306056.

[19] O. Dreyer, B. Krishnan, D. Shoemaker, and E. Schnetter, Phys. Rev. **D67**, 024018 (2003), gr-qc/0206008.

[20] M. Campanelli and C. O. Lousto, Phys. Rev. **D59**, 124022 (1999), arXiv:gr-qc/9811019 [gr-qc].

[21] T. Damour, P. Jaranowski, and G. Schafer, Phys. Rev. **D77**, 064032 (2008), arXiv:0711.1048 [gr-qc].

[22] A. Buonanno, Y. Chen, and T. Damour, Phys. Rev. **D74**, 104005 (2006), gr-qc/0508067.

[23] C. O. Lousto and Y. Zlochower, Phys. Rev. **D89**, 021501 (2014), arXiv:1307.6237 [gr-qc].

[24] M. Campanelli, C. O. Lousto, H. Nakano, and Y. Zlochower, Phys. Rev. **D79**, 084010 (2009), arXiv:0808.0713 [gr-qc].

[25] E. Barausse and L. Rezzolla, Astrophys. J. Lett. **704**, L40 (2009), arXiv:0904.2577 [gr-qc].

[26] C. O. Lousto and Y. Zlochower, Phys. Rev. **D89**, 104052 (2014), arXiv:1312.5775 [gr-qc].

[27] L. Blanchet, Living Rev.Rel. **17**, 2 (2014), arXiv:1310.1528 [gr-qc].

[28] G. Schfer, AIP Conf.Proc. **1577**, 132 (2014).

[29] M. Campanelli, C. O. Lousto, and Y. Zlochower, Phys. Rev. **D74**, 084023 (2006), astro-ph/0608275.

[30] E. Racine, Phys. Rev. **D78**, 044021 (2008), arXiv:0803.1820 [gr-qc].

[31] M. Campanelli, C. O. Lousto, Y. Zlochower, B. Krishnan, and D. Merritt, Phys. Rev. **D75**, 064030 (2007), gr-qc/0612076.

[32] Note that while the gravitational radiation time scale is $\sim r^4$, the flip-flop time scale is $\sim r^3$ (it is a conservative leading term).

[33] C. Nixon, A. King, and D. Price, (2013), arXiv:1307.0010 [astro-ph.HE].

[34] S. C. Noble, B. C. Mundim, H. Nakano, J. H. Krolik, M. Campanelli, Y. Zlochower, and N. Yunes, Astrophys. J. **755**, 51 (2012), arXiv:1204.1073 [astro-ph.HE].

[35] J. P. Leahy and P. Parma, in *Extragalactic Radio Sources. From Beams to Jets*, edited by J. Roland, H. Sol, and G. Pelletier (1992) pp. 307–308.

[36] M. Kesden, U. Sperhake, and E. Berti, Astrophys. J. **715**, 1006 (2010), arXiv:1003.4993 [astro-ph.CO].

[37] E. Berti, M. Kesden, and U. Sperhake, Phys. Rev. **D85**, 124049 (2012), arXiv:1203.2920 [astro-ph.HE].

[38] D. Gerosa, M. Kesden, E. Berti, R. O'Shaughnessy, and U. Sperhake, Phys. Rev. **D87**, 104028 (2013), arXiv:1302.4442 [gr-qc].